Reaction Modelling and Geometry Optimisation for Multi-tubular Membrane Catalytic Ammonia Cracker

Siyu Guo[a], Ziheng Zhao[b] and Mehmet Mercangöz[c]

[a] *Imperial College London, London, United Kingdom, siyu.guo18@imperial.ac.uk CA*
[b] *Imperial College London, London, United Kingdom, ziheng.zhao22@imperial.ac.uk*
[c] *Imperial College London, London, United Kingdom, m.mercangoz@imperial.ac.uk*

Abstract:
This study presents an NSGA-II-based optimisation framework for the design of a multi-tubular catalytic membrane reactor for hydrogen production via ammonia decomposition, with a focus on transportation applications. A reaction–separation model is developed to describe ammonia cracking and continuous hydrogen removal through a palladium membrane. The integrated membrane reactor enables high ammonia conversion under milder operating conditions than conventional packed-bed thermal cracking. Based on this mechanistic model, a multi-objective optimisation problem is formulated to analyse the trade-off between hydrogen productivity per reactor volume and per catalyst mass, using reactor geometry and operating conditions as decision variables. The resulting Pareto front identifies designs favouring either compactness or catalyst efficiency. In particular, long, slender reactors favour volumetric productivity, whereas shorter, wider reactors improve catalyst utilisation. Sensitivity analysis further shows strong temperature dependence and reduced conversion performance at high feed flow rates. Overall, the study demonstrates that combining mechanistic reactor modelling with multi-objective optimisation can support the rational design of membrane-integrated ammonia crackers for hydrogen energy systems.

Keywords:
Ammonia decomposition, Catalytic membrane reactor, Hydrogen production, Reactor optimisation, NSGA-II, Multi-objectives optimisation

1. Introduction

Decarbonising transportation remains difficult because aviation and maritime systems require high energy density fuels and are not readily electrified [1,2]. Hydrogen is an attractive carbon-free energy carrier, but its practical use is hindered by storage and transport challenges, including low volumetric energy density and demanding pressure or cryogenic requirements [3, 4]. Ammonia has therefore emerged as a promising hydrogen carrier because it is carbon-free, has high volumetric hydrogen density, and is easier to store and distribute than molecular hydrogen [5, 6].

Hydrogen can be released from ammonia through catalytic decomposition. A key challenge is achieving high conversion and hydrogen purity under conditions suitable for transport applications. Palladium-based membranes are attractive because of their high hydrogen selectivity and permeability [7, 8]. When integrated into catalytic membrane reactors (CMRs), they enable simultaneous reaction and separation, shifting the equilibrium toward ammonia decomposition and improving hydrogen yield [9–11].

This work builds on the multitubular catalytic membrane reactor (MTCMR) design reported by Guo et al. [12] and focuses on geometry optimisation for compact and efficient hydrogen production. For mobility applications, reactor volume and catalyst inventory are both critical; compact systems are desirable in aviation, whereas catalyst-efficient designs may be more attractive in maritime applications. We therefore formulate a multi-objective optimisation problem to maximise hydrogen produc-

tivity per reactor volume and per catalyst mass using five decision variables: inlet temperature, inlet pressure, inner diameter, outer diameter, and reactor length.
The optimisation is performed using NSGA-II, which is well suited to nonlinear multi-objective design problems and provides a distributed Pareto front without gradient information [13–15]. The resulting solutions clarify the trade-off between compactness and catalyst utilisation, while sensitivity analyses assess the influence of temperature, pressure, and feed flow rate on reactor performance. Overall, the study shows how mechanistic reactor modelling combined with multi-objective optimisation can support the design of membrane-integrated ammonia crackers for future hydrogen energy systems.

2. Model development

2.1. Physical description

As shown in Fig. 1, a compact multi-tubular membrane reactor is investigated in this study. The reactor is divided by the membrane into the reaction zone and the separation zone [19]. Ammonia decomposition is represented by Eq.R1. In the configuration shown in Fig.1, ammonia enters the reaction zone, where it converts into hydrogen and nitrogen. At the same time, the generated hydrogen permeates through the palladium membrane into the inner tube due to the pressure gradient across the membrane, allowing for both product purification and a favourable shift in reaction equilibrium.

$$2\,NH_3 \longleftrightarrow N_2 + 3\,H_2 \tag{R1}$$

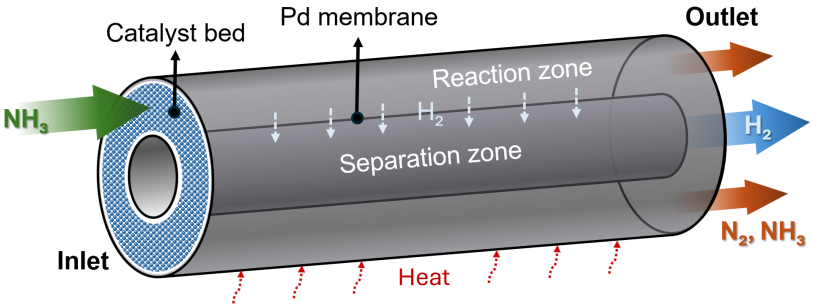

Figure 1: Schematic diagram of the catalytic multitubular membrane reactor adapted from Guo et al [12].

2.2. Model validation

A preliminary reactor design was used to assess model behaviour; the corresponding parameters are listed in Table **??**. The predicted ammonia conversion profile in Fig. **??** shows that conversion above 98.7% can be achieved at 450°C and 30 bar. This is considerably milder than conventional thermal cracking conditions and reflects the equilibrium enhancement created by continuous hydrogen permeation through the membrane.
Figure **??** further shows that reactor geometry becomes increasingly important as inlet flow rate rises. At low flow rates, high conversion is achieved over a broad range of diameter ratios. At higher flow rates, however, conversion exhibits a clear maximum with respect to geometry: increasing inner diameter initially improves permeation, but excessive enlargement reduces catalyst volume and penalises reaction performance. These results justify the need for geometry optimisation.

2.3. Optimisation problem definition

An optimisation study is performed to investigate two objective variables: the hydrogen production rate per reactor volume and (ii) the hydrogen production rate per catalyst mass, thereby assessing the enhancement potential of the membrane reactor according to specific process requirements. The first

objective reflects the volumetric productivity of the system, whereas the second objective indicates the catalyst utilisation ratio under identical feed conditions. Both metrics are essential for transportation applications, although their relative importance varies by sector. For instance, aviation places strict constraints on equipment volume and may therefore prioritise volumetric productivity, while maritime applications typically involve significantly higher fuel consumption. In such cases, minimising catalyst usage due to its high cost is more critical than reducing reactor volume.

The optimised design and operating variables in this study include the inner diameter of the inner tube d_{in}, the diameter of the outer tube d_{out}, and the reactor length L, which together determine the geometric configuration and membrane surface area available for hydrogen extraction. The inlet temperature T_{in} and inlet pressure P_{in} were selected as decision variables to capture the influence of thermodynamic driving forces and reaction kinetics on system performance. These five optimisation variables collectively govern the mass transfer, reaction rate, and separation efficiency within the membrane reactor.

The optimisation of these design and operating conditions was conducted using the second version of the non-dominated sorting genetic algorithm (NSGA-II). This algorithm is selected for its robust handling of complex, non-linear, and multi-objective problems, as well as its ease of integration with the developed reactor model. NSGA-II efficiently explores trade-offs between conflicting performance objectives while respecting operational constraints. The generic formulation of the optimisation problem is expressed as, where $\dot{n}_{H_2}$ is the production rate of hydrogen, $V_{reactor}(X)$ and $m_{cat}(X)$ are the corresponding reactor segment of volume and catalyst mass:

$$\text{Maximise: } \mathbf{F}(\mathbf{x}) = \begin{bmatrix} \dot{n}_{\mathrm{H_2}}/V_{\mathrm{reactor}}(\mathbf{x}) \\ \dot{n}_{\mathrm{H_2}}/m_{\mathrm{cat}}(\mathbf{x}) \end{bmatrix} \tag{1}$$

$$\text{Subject to: } \begin{cases} 0.01 \leq d_{\mathrm{in}} \leq 0.15 & \text{[m]} \\ 0.01 \leq d_{\mathrm{out}} \leq 0.15 & \text{[m]} \\ 0.05 \leq L \leq 1.00 & \text{[m]} \\ 530.0 \leq T_{\mathrm{in}} \leq 730.0 & \text{[K]} \\ 0.1 \leq P_{\mathrm{in}} \leq 3.0 & \text{[MPa]} \end{cases} \tag{2}$$

$$\text{with } \mathbf{x} = \left[d_{\mathrm{in}},\ d_{\mathrm{out}},\ L,\ T_{\mathrm{in}},\ P_{\mathrm{in}}\right] \tag{3}$$

2.4. Multi-objective optimisation

The NSGA-II algorithm begins by initialising decision variables with preliminary values. These variables serve as inputs to the equilibrium model. The algorithm evaluates results and assigns each a ranking using fast non-dominated sorting to identify Pareto fronts. After ranking, NSGA-II selects the best individuals for reproduction by prioritising those with lower ranks while considering crowding distance to explore more possibilities. These selected individuals then reproduce through crossover and mutation, simulating evolution and creating new offspring with decision variables. The new offspring are once again combined with the parental population, and the process repeats, gradually converging towards an optimised set of decision variables. Each full cycle of evaluation, ranking, selection, and reproduction in the evolutionary process is called a generation [13]. A route map is shown in Fig. 2 to illustrate the process. In this research, the initial population size is set to 50, and the termination condition is either the maximum number of generations reaches 50, or the number of stalled generations reaches 20.

To ensure a fair and meaningful optimisation, both objective functions are normalised to obtain comparable influence in the numerical solver. Since these metrics have inherently different units and

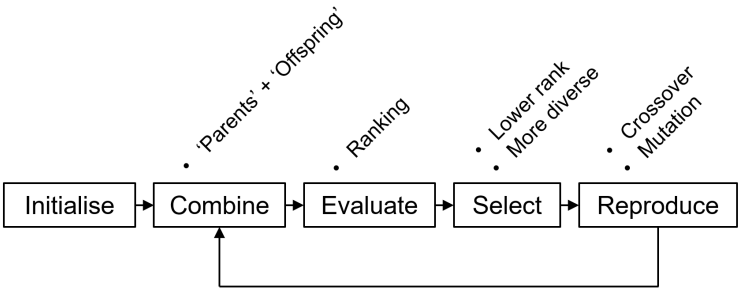

Figure 2: Flow chart of NSGA-II optimisation algorithm.

magnitudes, direct evaluation would bias the optimisation toward whichever metric numerically dominates. Therefore, before running optimisation, each objective was independently normalised using its respective maximum value obtained from preliminary simulations. This step aligns the two performance indicators on a common scale from 0 to 1, ensuring neither objective overshadows the other during trade-off evaluation. As a result, equal weighting in the multi-objective framework genuinely reflects equal design priority between maximising hydrogen extraction efficiency per reactor volume and per catalyst utilisation.

Following normalisation, a weighting coefficient was applied to each objective function to further balance its contribution relative to the penalty terms introduced for constraint handling. This coefficient ensures that maximising both objectives remains the dominant driver in the optimisation, while still allowing operational and design constraints to be adequately enforced. By tuning these coefficients, the optimisation algorithm maintains numerical stability and avoids scenarios where penalties either overwhelm the performance objectives or become insignificant. This scaling approach ensures that both objectives and penalties coexist within a meaningful range, enabling robust and unbiased identification of optimal reactor configurations. It also allows adjustments to the weighting of objectives in subsequent research. The calculations are carried out on a personal laptop with a 20-core, 13th Gen Intel(R) Core(TM) i7-13650HX CPU and 16 GB of RAM.

2.5. Optimisation results and discussion

Fig.3 represents the two objective functions - hydrogen production rate per unit catalyst mass and per unit reactor volume over 50 generations of NSGA-II. A rapid drop in objective values during the first 5-10 generations indicates that the algorithm is extremely efficient at identifying feasible designs with significantly improved hydrogen productivity. For generations beyond about the 10th, both curves start to level off, reflecting solutions approaching a near-optimum, stable Pareto region. No further improvement is observed beyond approximately 30 generations for each objective; hence, the optimum has been achieved to the limit of the algorithm. It should be noted that the objectives are negative values because NSGA-II is a minimisation-based algorithm; maximising hydrogen productivity was implemented in the code by minimising the negative of these performance metrics. After taking the opposite number, the penalties are added. Therefore, smaller values correspond to more favourable reactor designs. The average decision variables of the final population are reported in Table.1. The temperature and pressure always reach the upper boundary, which makes sense, as the reaction itself favours high temperature, and higher pressure allows more hydrogen to permeate across the membrane, further driving the reaction equilibrium forward.
Fig.4 presents the final Pareto front obtained from the NSGA-II optimisation, illustrating the trade-off between hydrogen permeation per unit catalyst mass and per unit reactor volume. The generally smooth, continuous distribution of non-dominated points demonstrates that NSGA-II explores the feasible region and converges to a well-defined set of optimal solutions. The overall curvature of the front reflects the progressive compromise between volumetric and catalyst-specific hydrogen productivity – gains in one objective necessarily come at the expense of the other, and the slope of the curve

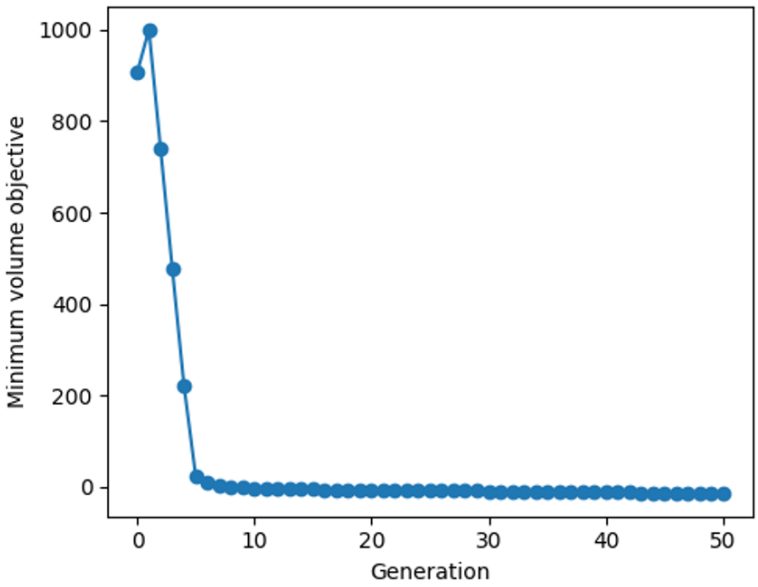

(a) Volume objective convergence status over 50 generations.

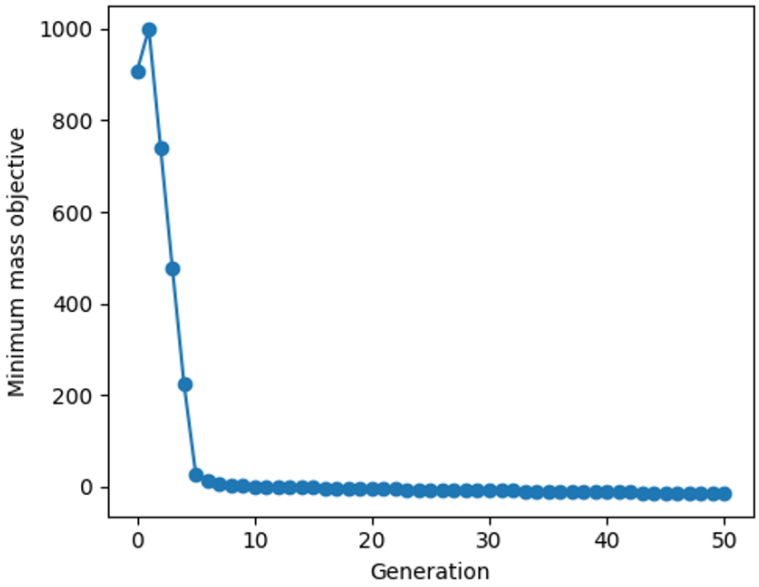

(b) Mass objective convergence status over 50 generations.

Figure 3: The convergence of the two objective functions with penalties included.

is an indicator of the sensitivity of each metric to such a trade-off. Regions characterised by a slope correspond to regimes where a gain in one objective can be achieved with relatively low penalties in the other, while at both extremes of slope, either very steep or very flat, reflect poor exchange rates between the objectives, meaning one must give up a lot in one metric to gain very little in the other.

Within this frontier, two distinct regions are observed, marked by great changes in slope. Both knees represent extreme points - one nearly vertical and the other nearly horizontal. The upper knee corresponds to designs that achieve exceptionally high hydrogen productivity per unit catalyst mass but only moderate volumetric efficiency; beyond this point, further improvements in catalyst-specific performance become nearly unattainable. On the other hand, the lower knee represents configurations that maximise hydrogen permeation per reactor volume, where even marginal gains in volumetric productivity are almost impossible to achieve. Such knee points are well established in multi-objective optimisation as boundaries of optimal trade-off solutions, indicating where the balance between conflicting objectives shifts from beneficial to diminishing returns. They thus provide a rational basis for selecting practical reactor geometries depending on whether catalyst utilisation or reactor compact-

Decision variable	Value
Outer diameter [m]	0.1085
Inner diameter [m]	0.0810
Reactor tube length [m]	0.5602
Operating temperature [K]	730.0 (Upper boundary)
Operating pressure [MPa]	3.0 (Upper boundary)

Table 1: Average optimised value of decision variables.

ness is the primary design priority. Analysis of the Pareto-optimal reactor geometries shows a linear

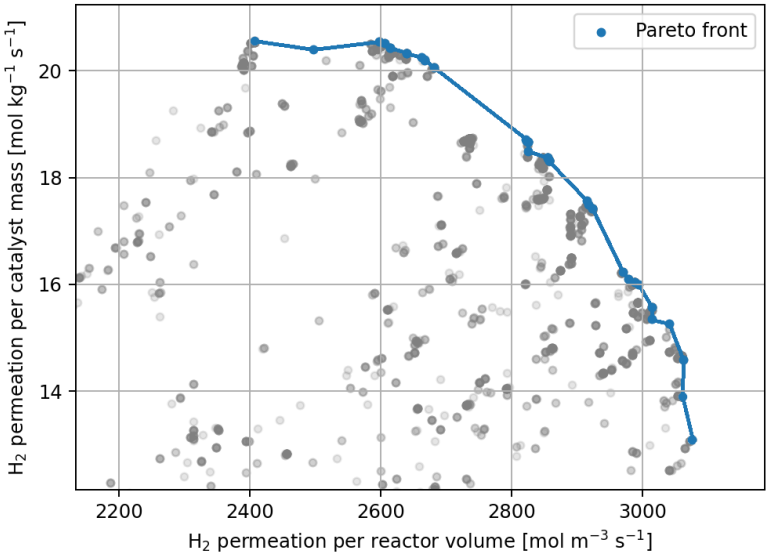

Figure 4: Pareto front of the membrane reactor hydrogen production rate from NSGA-II.

relationship between reactor length L and outer diameter d_{out} as shown in Fig.5. It can be observed that among Pareto-optimal geometries, as length increases, diameter decreases accordingly. This dimensional shift reduces the total reactor volume, since the quadratic decrease in diameter outweighs the linear increase in length. At the same time, the catalyst mass increases as the annular catalyst region widens and the reactor becomes longer. Consequently, longer, slimmer reactors result in a higher hydrogen production rate per unit volume but a lower rate per unit catalyst mass. This confirms that long, slim geometries are favoured when the volumetric objective is emphasised, and, conversely, short, wide designs are favoured when the catalyst mass objective is weighted more.

Following the discussion of how prioritising one objective over the other affects the optimal reactor geometry, the impact of applying different weightings to the two objectives is further investigated. The results shown in Fig.6 further illustrate how variation in the relative importance of the two objectives systematically shifts the optimiser towards different parts of the design space. Thus, giving more weight to catalyst-mass efficiency (red curve) favours designs that minimise catalyst use, even if this involves larger reactor volumes, whereas increasing weighting volumetric efficiency (green curve) drives the optimiser toward compact geometries that maximise hydrogen production per unit volume, at increased catalyst demand. Both optimisations converge under the same optimiser, demonstrating that NSGA-II is highly robust to such optimisation problems. This further reinforces that the preferred reactor configuration depends on context. While both objectives are clearly relevant to transportation systems, their relative importance varies across sectors. Aviation, for instance, is typically extremely volume-constrained and may prefer volumetric productivity, while maritime applications, with much higher fuel throughput, may prioritise minimising catalyst consumption due to its relatively high cost.

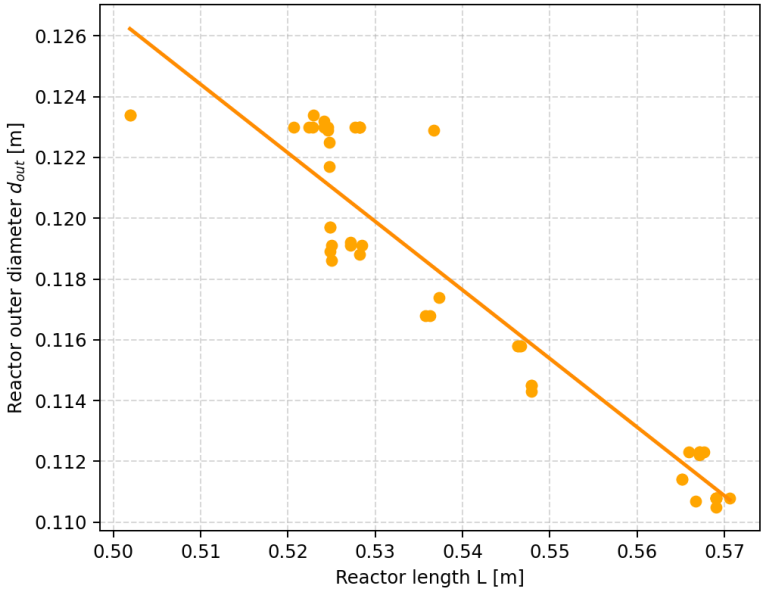

Figure 5: Length and diameter of Pareto-optimal insights.

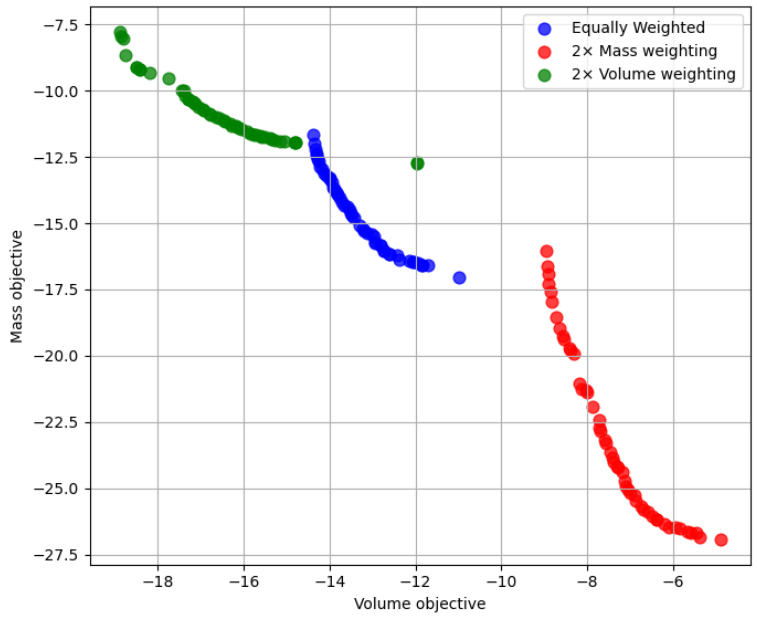

Figure 6: Pareto fronts of objective functions at different weightings.

2.6. Reactor Sensitivity Analysis

Sensitivity analysis is critical for evaluating reactor robustness and verifying design adequacy across a range of operating conditions. By systematically varying key parameters, it enables a clear understanding of reactor performance depends on its operating environment and how resilient the system remains under off-design or extreme scenarios. In the present study, temperature, pressure, and ammonia inflow rate are selected as the principal variables influencing the ammonia conversion profile. Examining their individual and combined impacts allows us to determine whether the reactor can consistently sustain high conversion efficiency and operational stability despite fluctuations or deviations from nominal conditions. This analysis ultimately supports the validation of the proposed reactor model and informs guidelines for safe and reliable operation.

The temperature-sensitivity analysis demonstrated in Fig.7 shows its strong influence on ammonia conversion in the tubular reactor. As the temperature increases from 623 K to 773 K, the conversion profile shows a significant increase in both the conversion rate and the overall conversion at the reactor outlet. At lower temperatures (573–623 K), conversion remains negligible across the entire reactor length, indicating that the reaction rate is insufficient to drive meaningful cracking even over 0.6 m of catalyst bed. At moderate temperatures (673–693 K), conversion increases approximately linearly along the reactor and reaches approximately 90% at the outlet. The most significant enhancement occurs at 723–773 K, where the reaction transitions into a kinetically favourable regime; ammonia conversion rapidly approaches 100% conversion. At 773 K in particular, conversion approaches completion over the optimal length. These results confirm that reactor performance is highly sensitive to temperature and that achieving high ammonia conversion requires operation within the upper thermal range of the design envelope. A similar trend is demonstrated in various past literature sources [12, 17, 18]. This insight is critical for establishing optimal operating conditions and ensuring sufficient hydrogen production even in the presence of temperature fluctuation during the operation.

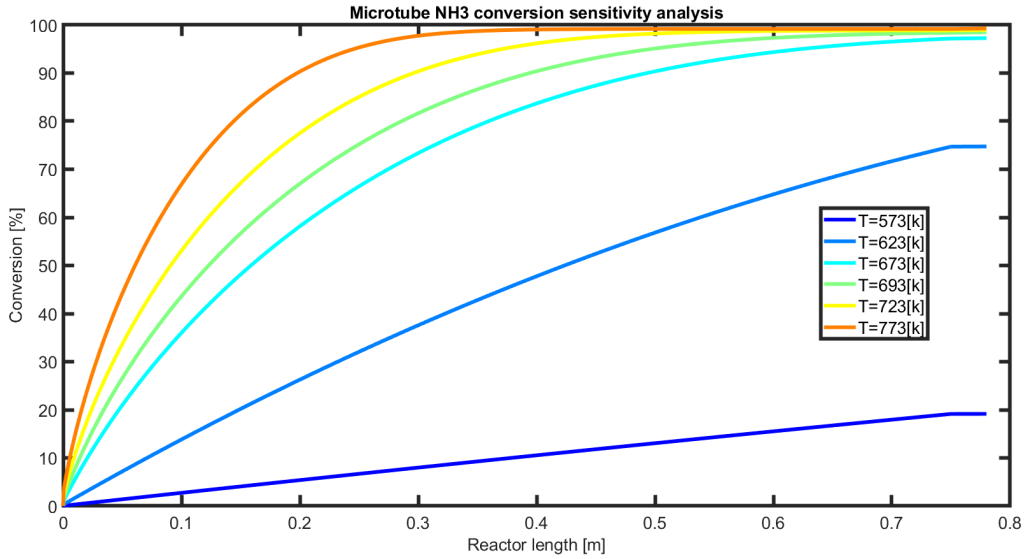

Figure 7: Ammonia conversion sensitivity analysis with variation on operating temperature varying from 623-753 K.

The sensitivity analysis of the ammonia inlet flow rate, as shown in Fig.8, reveals an inverse relationship between the feed rate and the conversion rate along the reactor. Although all examined flow rates ultimately approach similar final conversion levels near the reactor outlet, the trajectory by which they reach this point differs substantially. Lower inlet flow rates (e.g. 5.0-7.5 mol/s) exhibit a markedly steeper conversion gradient, achieving more than 90% conversion within the first 0.2–0.3 m of reactor length. This indicates that, under reduced throughput, the residence time and local reaction conditions are highly favourable, enabling rapid ammonia cracking with minimal reactor volume. Conversely, as inlet flow increases, the conversion curve becomes progressively flatter. Higher flow rates (12.5–15.0 mol/s) require nearly the full reactor length to reach comparable conversion, reflecting the diminishing residence time and reduced kinetic driving force available under high-throughput operation. This behaviour has important operational implications. While the reactor delivers high conversion across

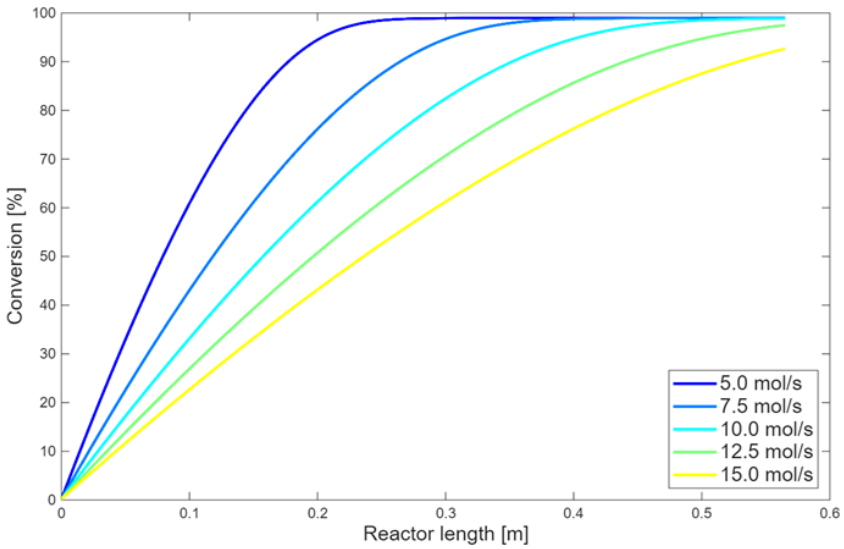

Figure 8: Ammonia conversion sensitivity analysis with different ammonia inlet flowrate varying from 5-15 mol/sec.

the full range of flow rates tested, the substantial reduction in conversion at elevated inlet flow rates introduces potential control challenges during periods of extreme hydrogen demand. Under such conditions, the reactor may struggle to reach the required conversion level quickly enough, leading to temporary underperformance or the need for supplemental control strategies such as dynamic temperature adjustment, flow modulation, or buffer storage. The findings highlight the need for a robust control system capable of compensating for the sensitivity of the conversion dynamics to inlet flow rate.

3. Conclusions

This work has developed and applied a coupled reaction-separation model and a multi-objective optimisation framework for the design of a multi-tubular catalytic membrane ammonia cracker. An equilibrium-based reactor model is formulated that captures the essential features of ammonia thermal decomposition, predicts high ammonia conversions in good agreement with literature trends [12], and demonstrates the strong equilibrium enhancement from continuous hydrogen removal via a palladium membrane. These results confirm that membrane-assisted ammonia cracking can achieve near-complete conversion under milder conditions than those required by conventional thermal reactors, supporting its suitability for hydrogen generation from ammonia in transport applications.

The reactor model is then optimised using NSGA-II for two objectives – hydrogen permeation rate per unit reactor volume and rate per unit catalyst mass, subject to five decision variables. The algorithm converged for the optimisation problem and moved to a smooth Pareto front, reporting a set of optimised decision variables. Additional analyses are conducted to evaluate the robustness of the optimisation under different objective weightings. The results show that NSGA-II performs consistently and reliably on this reactor design problem, demonstrating strong potential for application to other complex reactor optimisation problems.

4. Outlook

Future work will focus on strengthening the applicability, and engineering robustness of the reactor model through both expanded simulation studies and system-level integration. In terms of reactor modelling, further simulations will investigate the influence of catalyst-bed voidage and radial temperature profiles on conversion behaviour and membrane performance. These analyses will support

determining the reactor's operating envelope and provide validation against expected physical trends. Extending the current steady-state framework to a full dynamic model is a critical step, as a robust dynamic model enables transient behaviour, start-up/shutdown characteristics, and control-relevant sensitivities to be assessed. To complement one-dimensional modelling, a CFD simulation using COMSOL could be undertaken to evaluate local transport phenomena, non-uniformities, and potential design bottlenecks that reduced-order models cannot capture.

Beyond the reactor itself, the next phase of research should incorporate thermal management and process integration through a heat-exchanger network design. This could ensure that energy recovery, heat duties, and thermal coupling are accurately represented.

Insights from the sensitivity analysis also reveal several areas that require attention. First, safety and economic constraints were insufficiently represented in the current optimisation setup. Preliminary findings indicate that the selected membrane surface area may be excessively large, potentially resulting in triggering reverse permeation of hydrogen under certain conditions. Moreover, the pressure difference between the inner and outer tubes raises structural concerns regarding membrane tolerance. On the retentate side, the limited cross-sectional area of the outer tube may impose risks such as choked flow. Addressing these issues will require more robust NSGA-II constraint formulations that reflect realistic mechanical limits, operability considerations, and capital costs. Improving the formulation ensures future optimisation outputs are aligned with practical engineering feasibility.

Acknowledgments

The author would like to express sincere gratitude to the Sargent Centre for Process Systems Engineering, Imperial College London, for providing all necessary licenses for the simulation tools used in this study.

Nomenclature

Roman letters

r_{NH_3} Reaction rate, $\mathrm{mol\,s^{-1}\,m^{-3}}$
p_i Partial pressure of component i, Pa
k_{eq} Equilibrium constant, $-$
M_i Molar mass of component i, $\mathrm{kg/mol}$
M_{mix} Average molar mass of mixture, $\mathrm{kg/mol}$
x_i Molar fraction of component i, $-$
T Temperature, K
k Reaction kinetic constant, $-$
$D_{k,m}$ Knudsen diffusion coefficient of mixture, $-$
$D_{p,m}$ Knudsen + binary diffusion coefficient of mixture, $-$
$D_{p0,m}$ Intermediate variable for Knudsen diffusion calculation, $-$
P Reactor pressure, Pa
R Universal gas constant, 8.314
r_{av} Correction parameter, 1×10^{-6}
h_T Thiele modulus, $-$
Q_{H_2} H_2 permeation rate of hydrogen, $\mathrm{mol\,m^{-2}\,s^{-1}}$
r_p Catalyst particle diameter, m
$\dot{m}$ Mass flow rate, $\mathrm{kg/s}$
u_0 Gas superficial velocity, $\mathrm{m/s}$
A_{cs} Cross sectional area of reactor unit, $\mathrm{m^2}$

$\dot{n}_{H_2}$ H_2 permeation rate, $\mathrm{mol\,s^{-1}}$

V_{reactor} Volume of single reactor unit, $\mathrm{m^3}$

m_{cat} Mass of catalyst load, kg

Greek symbols

η Catalyst efficiency factor, $-$

$\sigma^2_{mix}\omega_{mix}$ Acentric factor of mixture, an intermediate variable, $-$

ν Intermediate variable related to viscosity, $-$

μ_i Viscosity of component i, $\mathrm{Pa \cdot s}$

μ_{mix} Viscosity of the mixture, $\mathrm{Pa \cdot s}$

ϵ Catalyst bed voidage, 0.7

τ_{solid} Catalyst tortuosity factor, 4

ρ_{solid} Catalyst bulk density, $\mathrm{kg\,m^{-3}}$

ρ_p Catalyst particle density, $\mathrm{kg\,m^{-3}}$

ρ_{mix} Density of gas mixture, $\mathrm{kg\,m^{-3}}$

β Exponential constant in rate law, $-$

Φ_{ij} Molecular interaction parameter, $-$

Subscripts and superscripts

i Chemical component, consisting of ammonia (NH_3), hydrogen (H_2), and nitrogen (N_2)

mix Gas mixture, corresponding to hydrogen, nitrogen, and ammonia

References

[1] International Energy Agency. *CO2 Emissions – Global Energy Review 2025*. Available at: `https://www.iea.org/reports/global-energy-review-2025/co2-emissions` [accessed 09.12.2025].

[2] Lutsey N., Sperling D. *Greenhouse gas mitigation supply curve for the United States for transport versus other sectors*. Transportation Research Part D: Transport and Environment 2009;14(3):222–229.

[3] Wang N., Huang S., Zhang Z., Li T., Yi P., Wu D., Chen G. *Laminar burning characteristics of ammonia/hydrogen/air mixtures with laser ignition*. International Journal of Hydrogen Energy 2021;46(62):31879–31893.

[4] Di Carlo A., Dell'Era A., Del Prete Z. *3D simulation of hydrogen production by ammonia decomposition in a catalytic membrane reactor*. International Journal of Hydrogen Energy 2011;36(18):11815–11824.

[5] Moudio N.D.N., Bian X.-Q., Chinamo D.S. *Liquid hydrogen carriers for clean energy systems: A critical review of chemical hydrogen storage strategies*. Fuel 2026;404:136329.

[6] Valera-Medina A., Xiao H., Owen-Jones M., David W.I.F., Bowen P.J. *Ammonia for power*. Progress in Energy and Combustion Science 2018;69:63–102.

[7] Cerone N., Zito G.D., Florio C., Fabbiano L., Zimbardi F. *Recent advancements in Pd-based membranes for hydrogen separation*. Energies 2024;17(16):4095.

[8] Conde J.J., Maroño M., Sánchez-Hervás J.M. *Pd-based membranes for hydrogen separation: review of alloying elements and their influence on membrane properties*. Separation & Purification Reviews 2017;46(2):152–177.

[9] Zhang X., Li C., He Z., Han T. *Integration of ammonia synthesis gas production and N2O decomposition into a membrane reactor*. Industrial & Engineering Chemistry Research 2020;60(7):3066–3072.

[10] Cechetto V., Di Felice L., Gallucci F. *Advances and Perspectives of H2 production from NH3 decomposition in membrane reactors*. Energy & Fuels 2023;37(15):10775–10798.

[11] Maccarrone D., Giorgianni G., Italiano C., Perathoner S., Centi G., Abate S. *Comparative analysis of hydrogen production from ammonia decomposition in membrane and packed bed reactors using diluted NH3 streams*. International Journal of Hydrogen Energy 2024;82:513–522.

[12] Guo S., Mercangöz M. *Design and Evaluation of a Multitubular Catalytic Membrane Reactor for Onboard Ammonia Cracking in Commercial Aviation*. ASME Open Journal of Engineering 2025;4.

[13] Deb K., Pratap A., Agarwal S., Meyarivan T. *A fast and elitist multiobjective genetic algorithm: NSGA-II*. IEEE Transactions on Evolutionary Computation 2002;6(2):182–197.

[14] Konak A., Coit D.W., Smith A.E. *Multi-objective optimization using genetic algorithms: A tutorial*. Reliability Engineering & System Safety 2006;91(9):992–1007.

[15] Coello C.A.C. *Evolutionary multi-objective optimization: a historical view of the field*. IEEE Computational Intelligence Magazine 2006;1(1):28–36.

[16] Collins J.P., Way J.D., Kraisuwansarn N. *A mathematical model of a catalytic membrane reactor for the decomposition of NH3*. Journal of Membrane Science 1993;77(2–3):265–282.

[17] Sima D., Wu H., Tian K., Xie S., Foo J.J., Li S., Wang D., Ye Y., Zheng Z., Liu Y.-Q. *Enhanced low temperature catalytic activity of Ni/Al–$Ce_{0.8}Zr_{0.2}O_2$ for hydrogen production from ammonia decomposition*. International Journal of Hydrogen Energy 2020;45(16):9342–9352.

[18] Mukherjee S., Devaguptapu S.V., Sviripa A., Lund C.R.F., Wu G. *Low-temperature ammonia decomposition catalysts for hydrogen generation*. Applied Catalysis B: Environmental 2018;226:162–181.

[19] Tang X.-Y., Yang W.-W., Ma X., Cao X.E. *An integrated modeling method for membrane reactors and optimization study of operating conditions*. Energy 2023;268:126730.